Femtosecond laser written optofluidic sensor: Bragg grating waveguide evanescent probing of microfluidic channel

Valeria Maselli,* Jason R. Grenier, Stephen Ho, and Peter R. Herman

University of Toronto, The Edward S. Rogers Sr. Department of Electrical and Computer Engineering and the Institute for Optical Sciences, 10 King's College Road, M5S 3G4 Toronto, Ontario, Canada.
*valeria.maselli@utoronto.ca

Abstract: Microfluidic channels and Bragg Grating Waveguides (BGWs) were simultaneously fabricated inside fused silica glass by means of femtosecond laser exposure followed by chemical etching. Evanescent field penetration of the waveguide mode into the parallel microfluidic channel induced Bragg resonant wavelength shifts to enable refractive index characterization of the fluidic medium in the 1 to 1.452 range. Laser exposure was optimized to fabricate devices with optically smooth channel walls and narrow Bragg resonances for high sensing response at 1560 nm wavelength. Reference gratings were also employed in the optical circuit for temperature and strain compensation. These devices open new directions for optical sensing in three-dimensional optofluidic and reactor microsystems.

OCIS codes: (130.3120) Integrated optics devices; (140.3390) Laser materials processing; (140.7090) Ultrafast lasers; (230.1480) Bragg reflectors; (280.4788) Optical sensing and sensors.

References and links

1. K. B. Mogensen, N. J. Petersen, J. Hübner, and J. P. Kutter, "Monolithic integration of optical waveguides for absorbance detection in microfabricated electrophoresis devices," Electrophoresis **22**, 3930–3938 (2001).
2. K. B. Mogensen, Y. C. Kwok, J. C. T. Eijkel, N. J. Petersen, A. Manz, and J. P. Kutter, "A Microfluidic Device with an Integrated Waveguide Beam Splitter for Velocity Measurements of Flowing Particles by Fourier Transformation," Anal. Chem. **75**, 4931–4936 (2003).
3. K. B. Mogensen, J. El-Ali, A. Wolff, and J. P. Kutter, "Integration of polymer waveguides for optical detection in microfabricated chemical analysis systems," Appl. Opt. **42**, 4072–4079 (2003).
4. S. Mandal and D. Erickson, "Nanoscale optofluidic sensor arrays," Opt. Express **16**, 1623–1631 (2008).
5. Y. Bellouard, A. Said, M. Dugan, and P. Bado, "Fabrication of high-aspect ratio micro-fluidic channels and tunnels using femtosecond laser pulses and chemical etching," Opt. Express **12**, 2120–2129 (2004).
6. G. T. A. Kovac, *Micromachined Transducers Sourcebook* (McGraw Hill, New York, 1998).
7. K. B. Mogensen, H. Klank, and J. P. Kutter, "Recent developments in detection for microfluidic systems," Electrophoresis **25**, 3498–3512 (2004).
8. D. Erickson, S. Mandal, A. H. J. Yang, and B. Cordovez, "Nanobiosensors: optofluidic, electrical and mechanical approaches to biomolecular detection at the nanoscale," Microfluidics and Nanofluidics **4**, 33–52 (2008).
9. A. Y. Fu, C. Spence, A. Scherer, F. H. Arnold, and S. R. Quake, "A microfabricated fluorescence-activated cell sorter," Nat. Biotechnol. **17**, 1109–1111 (1999).
10. E. Chow, A. Grot, L. W. Mirkarimi, M. Sigalas, and G. Girolami, "Ultracompact biochemical sensor built with two-dimensional photonic crystal microcavity," Opt. Lett. **29**, 1093–1095 (2004).
11. A. B. Matsko and V. S. Ilchenko, "Optical resonators with whispering-gallery modes - Part I: Basics," IEEE J. Sel. Top. Quantum Electron. **12**, 3–14 (2006).
12. B. J. Luff, J. S. Wilkinson, J. Piehler, U. Hollenbach, J. Ingenhoff, and N. Fabricius, "Integrated optical Mach-Zehnder biosensor," J. Lightwave Technol. **16**, 583–592 (1998).
13. R. Karlsson, "SPR for molecular interaction analysis: a review of emerging application areas," Journal of Molecular Recognition **17**, 151–161 (2004).
14. D. A. Pereira, O. Frazão, and J. L. Santos, "Fiber Bragg grating sensing system for simultaneous measurement of salinity and temperature," Opt. Eng. **43**, 299–304 (2004).

#111972 - $15.00 USD Received 27 May 2009; revised 11 Jun 2009; accepted 23 Jun 2009; published 26 Jun 2009

15. A. N. Chryssis, S. M. Lee, S. B. Lee, S. S. Saini, and M. Dagenais, "High Sensitivity Evanescent Field Fiber Bragg Grating Sensor," IEEE Photon. Technol. Lett. **17**, 1253–1255 (2005).
16. J. C. Gates, C. H. Holmes, F. R. M. Adikan, C. B. E. Gawith, and P. G. R. Smith, "New geometry for planar UV written refractive index sensors," Proc. SPIE **6585**, 65850O (2007).
17. C. Schaffer, A. Brodeur, J. García, and E. Mazur, "Micromachining bulk glass by use of femtosecond laser pulses with nanojoule energy," Opt. Lett. **26**, 93–95 (2001).
18. A. Marcinkevičius, S. Juodkazis, M.Watanabe, M. Miwa, S. Matsuo, H. Misawa, and J. Nishii, "Femtosecond laser-assisted three-dimensional microfabrication in silica," Opt. Lett. **26**, 277–279 (2001).
19. Y. Cheng, K. Sugioka, K. Midorikawa, M. Masuda, K. Toyoda, M. Kawachi, and K. Shihoyama, "Three-dimensional micro-optical components embedded in photosensitive glass by a femtosecond laser," Opt. Lett. **28**, 1144–1146 (2003).
20. C. Hnatovsky, R. S. Taylor, E. Simova, V. R. Bhardwaj, D. M. Rayner, and P. B. Corkum, "Polarization-selective etching in femtosecond laser-assisted microfluidic channel fabrication in fused silica," Opt. Lett. **30**, 1867–1869 (2005).
21. Y. Shimotsuma, P. Kazansky, J. Qiu, and K. Hirao, "Self-Organized Nanogratings in Glass Irradiated by Ultrashort Light Pulses," Phys. Rev. Lett. **91**, 247405 (2003).
22. K. Sugioka, Y. Cheng, and K. Midorikawa, "Three-dimensional micromachining of glass using femtosecond laser for lab-on-chip device manufacture," Appl. Phys. A **81**, 1–10 (2005).
23. R. W. Applegate Jr., J. Squier, T. Vestad, J. Oakey, D. W. M. Marr, P. Bado, M. A. Dugan, and A. A. Said, "Microfluidic sorting system based on optical waveguide integration and diode laser bar trapping," Lab Chip **6**, 422–426 (2006).
24. R. Osellame, V. Maselli, R. Martinez Vazquez, R. Ramponi, and G. Cerullo, "Integration of optical waveguides and microfluidic channels both fabricated by femtosecond laser irradiation," Appl. Phys. Lett. **90**, 231118 (2007).
25. M. Kim, D. J. Hwang, H. Jeon, K. Hiromatsu, and C. P. Grigoropoulos, "Single cell detection using a glass-based optofluidic device fabricated by femtosecond laser pulses," Lab Chip **9**, 311–318 (2009).
26. L. Shah, A. Y. Arai, S. Eaton, and P. Herman, "Waveguide writing in fused silica with a femtosecond fiber laser at 522 nm and 1 MHz repetition rate," Opt. Express **13**, 1999–2006 (2005).
27. H. Zhang, S. M. Eaton, and P. R. Herman, "Single-step writing of Bragg grating waveguides in fused silica with an externally modulated femtosecond fiber laser," Opt. Lett. **32**, 2559–2561 (2007).
28. R. Kashyap, *Fiber Bragg gratings* (Academic Press, San Diego, CA, 1999).
29. C. Hnatovsky, R. S. Taylor, E. Simova, P. P. Rajeev, D. M. Rayner, V. R. Bhardwaj, and P. B. Corkum, "Fabrication of microchannels in glass using focused femtosecond laser radiation and selective chemical etching," Appl. Phys. A **84**, 47–61 (2006).
30. V. Maselli, R. Osellame, G. Cerullo, R. Ramponi, P. Laporta, L. Magagnin, and P. L. Cavallotti, "Fabrication of long microchannels with circular cross section using astigmatically shaped femtosecond laser pulses and chemical etching," Appl. Phys. Lett. **88**, 191107 (2006).
31. S. Ho, M. L. Ng, S. M. Eaton, P. R. Herman, and J. S. Aitchison, "Single and Multi-Scan Femtosecond Laser Writing for Selective Chemical Etching of Glass Micro-Channels," in *Conference on Lasers and Electro-Optics/Quantum Electronics and Laser Science and Photonic Applications Systems Technologies*, (Optical Society of America, 2007), paper CThJ4, http://www.opticsinfobase.org/abstract.cfm?URI=CLEO-2007-CThJ4.
32. S. Ho, S. Eaton, M. L. Ng, J. S. Aitchison, and P. R. Herman, University of Toronto, 10 King's College Road, M5S 3G4 Toronto, Ontario, Canada, are preparing a manuscript to be called "Single- and multi-scan femtosecond laser writing for selective chemical etching of cross-section patternable glass micro-channels."
33. V. Maselli, "Femtosecond laser fabrication of optical waveguides and microfluidic channels," Ph.D. Thesis, Politecnico di Milano, Piazza Leonardo da Vinci, 32, 20133 Milano, Italy (2007).
34. K. C. Vishnubhatla, N. Bellini, R. Ramponi, G. Cerullo, and R. Osellame, "Shape control of microchannels fabricated in fused silica by femtosecond laser irradiation and chemical etching," Opt. Express **17**, 8685–8695 (2009).
35. H. Zhang, S. Ho, S. M. Eaton, J. Li, and P. R. Herman, "Three-dimensional optical sensing network written in fused silica glass with femtosecond laser," Opt. Express **16**, 14015–14023 (2008).
36. W. W. Morey, G. Meltz, and W. H. Glenn, "Bragg-grating temperature and strain sensors," in *Proceedings of the 6th International Conference on Optical Fiber Sensors* (Springer-Verlag, Paris, France, 1989), pp. 526–531.
37. A. Othonos, "Fiber Bragg gratings," Rev. Sci. Instrum. **68**, 4309–4341 (1997).

1. Introduction

Lab-on-chip (LOC) devices are revolutionizing various fields, both in basic research and in clinical applications as a low-cost diagnostic tool. LOCs are currently fabricated in silicon [1], glass [2] or polymer [3] materials using well-established techniques such as semiconductor processing, and photo- or soft-lithography [4]. The evolution for more functional LOC

#111972 - $15.00 USD Received 27 May 2009; revised 11 Jun 2009; accepted 23 Jun 2009; published 26 Jun 2009

systems has been towards three-dimensional (3D) devices formed in multistep processes [5] that include stacking and fusing of multilayer components [6]. In this trend, on-chip optical detection systems are desired to replace massive bench-top instrumentation currently required for fluorescence or absorption of analytes [7], label-free biomolecular detection [8], particle sorting [9] and various other optical sensing applications.

In such direction, on-chip optical monitoring of the refractive index of fluids or gases inside channels has been explored with photonic crystals [10], Fabry-Perot and other resonant cavities [11], interferometers [12], and evanescent probing by surface plasmon resonance (SPR) reflection [13]. Although not LOC devices, optical fibers conveniently relay light to fiber Bragg grating (FBG) sensors [14] which can be acid-thinned for highly sensitive evanescent probing up to 1394 nm/riu (riu: refractive index unit) response [15]. Gates *et al*. recently extended the FBG sensor concept to LOCs by UV laser writing of Bragg grating waveguides (BGWs) within a photosensitive silica layer positioned to intersect surface microchannels [16]. These integrated BGWs and microfluidics open more directions for developing highly functional and robust optofluidic microsystems without the packaging disadvantages of FBGs. However, embedded Bragg grating devices must be compensated for environment factors such as temperature and strain, and extension from planar to more flexible 3D systems is also greatly desirable to permit more complex processing on a chip.

Femtosecond laser direct writing inside the bulk of glass substrates has emerged as a simple, attractive, single-step approach for generating both 3D optical circuits [17] and modification tracks that can be chemically etched (hydrofluoric (HF) acid etching). For the latter, photochemical modification [18,19] or nanograting formation [20,21] facilitate differential etching rates as high as 100:1 to obtain high aspect ratio channels and 3D-patterned microfluidic networks buried inside bulk glasses. Exploiting the 3D capabilities of the femtosecond writing technique opens new avenues for dense integration of optical and microfluidic components that are not possible with open surface channel devices, while also facilitating simpler techniques for sealing channels. Photosensitivity mechanisms in Foturan glass were tailored by Sugioka *et al*. to fabricate and integrate Y-branched microchannels, micromechanical valves, and micro-optical components such as mirrors [22], while in fused silica optofluidic sensing devices have been laser-formed [23,24] including a single cell detector by Grigoropoulos and co-workers [25].

In this paper, we present the first example of microfluidic channels and Bragg grating waveguides co-fabricated inside fused silica glass by means of femtosecond laser writing and chemical etching. Laser polarization and exposure conditions were manipulated to inhibit HF etching of the BGWs and thereby facilitate close (<2 μm) placement of the waveguides parallel to very smooth microfluidic channels, formed below the glass surface. Laser writing and etching processes were tuned for strong optical response by means of narrow Bragg resonance linewidth (0.2 nm), formation of uniform and smooth channel walls, and device layout design. In this way, evanescent probing of the waveguide mode into the liquid-filled microchannel induced sufficient Bragg wavelength shift for characterization of refractive index in the 1 to 1.452 range. Reference gratings were also embedded into the substrate for temperature and strain compensation to improve sensor accuracy. These results present a new direction for optical sensing of gases, liquids, and biological media by novel 3D optofluidic microsystems made available by femtosecond laser processes.

2. Device fabrication

2.1 Experimental set-up

Fused silica was selected for the optofluidic platform to take advantage of its superior optical quality, exceptional transmittance over a wide spectral range (from 0.16 μm to 3 μm), low thermal expansion coefficient, high thermal stability and strong chemical resistance. The laser exposure set-up for writing both Bragg grating waveguides and modification tracks for HF etching is depicted in Fig. 1. An ultrafast fiber laser system (IMRA America, model: FCPA μJewel D400-VR) delivered pulses at 1045 nm wavelength with 500 kHz repetition rate and

#111972 - $15.00 USD Received 27 May 2009; revised 11 Jun 2009; accepted 23 Jun 2009; published 26 Jun 2009

~300 fs duration pulses through a power attenuator, consisting of a linear polarizer and a rotatable half-wave plate (HWP). An acousto-optic modulator (AOM; NEOS 23080-3-1.06-LTD) created laser bursts with 60% duty cycle and 500 Hz modulation frequency to form segmented waveguides. Focusing with lens L_1 into lithium triborate (LBO) crystal provided second-harmonic 522 nm light, which is more efficient for inscribing low-loss waveguides inside fused silica glasses [26]. After collimation by lens L_2 and filtering of the beam fundamental wavelength (short-pass filter: SP), turning mirrors (TM) directed the green beam through a choice of polarizers (*i.e.*, HWP) and into a 0.55 numerical aperture (NA) aspheric lens. A beam waist of ~1 μm spot size (1/exp(2) diameter) was formed 75 μm below the surface of the fused silica glass substrate (Corning 7980, 25 mm × 50 mm × 1 mm dimensions), mounted on a two-dimensional (2D) air bearing motion stage (Aerotech ABL1000, with 2 nm resolution and 50 nm repeatability) for precise computer-controlled scanning. The focusing lens was moved with a linear stage (Aerotech ALS130) to adjust the vertical focal position.

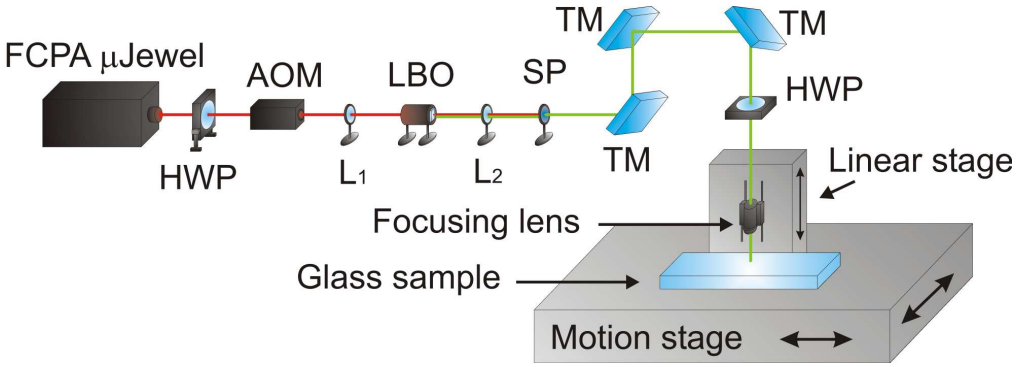

Fig. 1. Experimental set-up for femtosecond laser fabrication of Bragg grating waveguides and microfluidic channels.

2.2 Bragg grating waveguides

The acousto-optic modulator created laser bursts to form a continuous array of refractive index voxels that simultaneously provided low-loss waveguiding (~0.6 dB/cm), efficient mode coupling with standard optical fibers, and high-strength Bragg resonance (waveguide reflectance $R \approx 90\%$ and transmittance $T \approx$ -35 dB), as previously reported in [27]. The Bragg wavelength (λ_B) was controlled by [28]:

$$\lambda_B = 2n_{eff}\Lambda = 2n_{eff}v/f \qquad (1)$$

where Λ represents the grating period, v is the sample translation speed, f = 500 Hz is the AOM modulation frequency, and $n_{eff} \approx 1.445$ is the effective refractive index of the mode propagating inside the BGW. For an infrared resonance $\lambda_B \approx 1560$ nm, v = 0.26989 mm/s scan speed provided Λ = 539.78 nm Bragg period. An optimized 150 nJ pulse energy was used and the sample was translated in a direction parallel to the laser polarization to avoid birefringent waveguides.

2.3 Microfluidic channels

The laser polarization was oriented perpendicular to the sample translation direction to align the nanogratings parallel with the structure walls and thus facilitate deep HF etching of channels [20,21,29,30] with smooth vertical walls positioned adjacent to the waveguides. A scan speed of 0.5 mm/s and pulse energy of 80 nJ were used to create a 5 × 5 array of parallel modification tracks, with a layer-to-layer separation of 2 μm and a track-to-track separation of 1 μm, that led to formation of horizontal rectangular microchannels positioned 75 μm below

#111972 - $15.00 USD Received 27 May 2009; revised 11 Jun 2009; accepted 23 Jun 2009; published 26 Jun 2009

the glass surface [31]. Increased pulse energy or focusing depth, or slower scan speed, caused micro-crack formation due to stress accumulation, resulting in corrugated walls. Larger track-to-track spacing led to incomplete etching between tracks and increased sidewall roughness. An atomic force microscope (AFM) scan of channel walls revealed only ~10 nm (rms) vertical sidewall roughness on an area of 3 μm × 3 μm while 20-fold larger roughness, measured on an area of 50 μm × 50 μm, was seen on the bottom of the channel [32]. Greater area AFM scans were not possible for the sidewalls due to structural obstructions but only 2- to 3-fold larger roughness is anticipated. The stark difference in roughness for side and horizontal walls is attributed to the vertical orientation of nanograting planes that align with and define the smooth sidewalls after HF etching. The ends of the nano-planes on the top and bottom surfaces thus define raster-like scan lines that significantly increase the surface roughness. The AOM was not modulated during laser modification except to cut the laser beam at channel ends or corners, thereby reducing stress and crack formation due to overexposure.

A wide range of laser exposure and etching conditions were tested to minimize microchannel wall roughness and thus enable very close placement of the BGWs to the channels for high evanescent field penetration of the waveguide mode, while also inhibiting the etchant from breaking through to the waveguide core. Uniform sidewalls that remained parallel along the grating lengths were essential for a narrow Bragg resonance linewidth while smooth walls were important for preventing high optical mode scattering loss. Since acid depletion is known to cause significant channel tapering in long channels (up to ~2.6 mm single-side length) [33], the method of [32] was employed to generate a periodic array of vertical access holes to connect the sample surface to the buried laser tracks with multiple entry points for the etchant. The approach by Vishnubhatla *et al*. to use conically shaped spiraling modification tracks to form long (4 mm) and straight cylindrical channels was not tested here [34]. The vertical access holes were exposed at higher net dosage of 1 mm/s velocity and 200 nJ pulse energy to facilitate higher speed HF etching, and were evenly spaced at 100 μm intervals along the channel length.

After laser exposure of waveguide and channel tracks, the sample was immersed in a 10% aqueous HF solution for 2.5 hours. Higher HF concentration increased channel roughness, while lower concentration required significantly longer etching time. Figure 2(d) shows a top view of a microchannel formed parallel to a BGW prior (top) and after (bottom) HF etching. The expected nanograting planes are parallel to the channel walls, yielding a smooth interface with only 1.5 μm distance from the waveguide. The minimum gap was found by reducing the BGW-to-channel separation distance in 250 nm steps until the HF broke through into the BGW. The 5 × 5 arrayed modification tracks were completely opened by the HF acid, and doubled in size from an original ~5.5 μm wide modification structure to an ~11 μm wide channel. Under the present optical microscope resolution, tapering of the channel between the two consecutive access holes (100 μm apart) is not apparent for these optimized laser exposure conditions. The inset figure (bottom right of Fig. 2(d)) shows the 12 μm diameter access hole when imaging onto the sample surface. When using circular or parallel laser polarization during laser writing, the channel walls were significantly rougher, etching was incomplete, and the BGWs could not be placed sufficiently close to the microfluidic channels without HF etching into the waveguides.

3. Microfluidic systems

Three different optofluidic device geometries, depicted in Fig. 2 (a-c), were tested in this work. The first topology (Fig. 2(a)) consisted of a straight BGW formed parallel to a shorter microchannel. The 25 mm long BGW was composed of three serially cascaded segments, each one with a distinct Bragg wavelength represented in the schematic by a different color. The sensing grating in the middle (yellow) was positioned close and matched axially to the 10 mm length of the channel. This sensor grating was sandwiched by two 7.5 mm long reference grating waveguides (green and pink in Fig. 2(a)), which were used as a gauge for

#111972 - $15.00 USD Received 27 May 2009; revised 11 Jun 2009; accepted 23 Jun 2009; published 26 Jun 2009

temperature or strain compensation during the refractive index characterization. The reference grating Bragg resonances $\lambda_1 = 1530$ nm and $\lambda_3 = 1550$ nm were positioned on the short wavelength side of the sensor grating resonance $\lambda_2 = 1560$ nm, in order to avoid radiation mode loss at the sensing wavelength. The three different BGWs were generated by abruptly changing the sample scan speed (0.26471 mm/s, 0.26989 mm/s and 0.26815 mm/s, respectively for λ_1, λ_2 and λ_3) during laser writing. The microscope image of Fig. 2(d) shows a 1.5 μm separation of the channel from the BGW, representing the thinnest 'stop-layer' observed here without HF break-through into the waveguide.

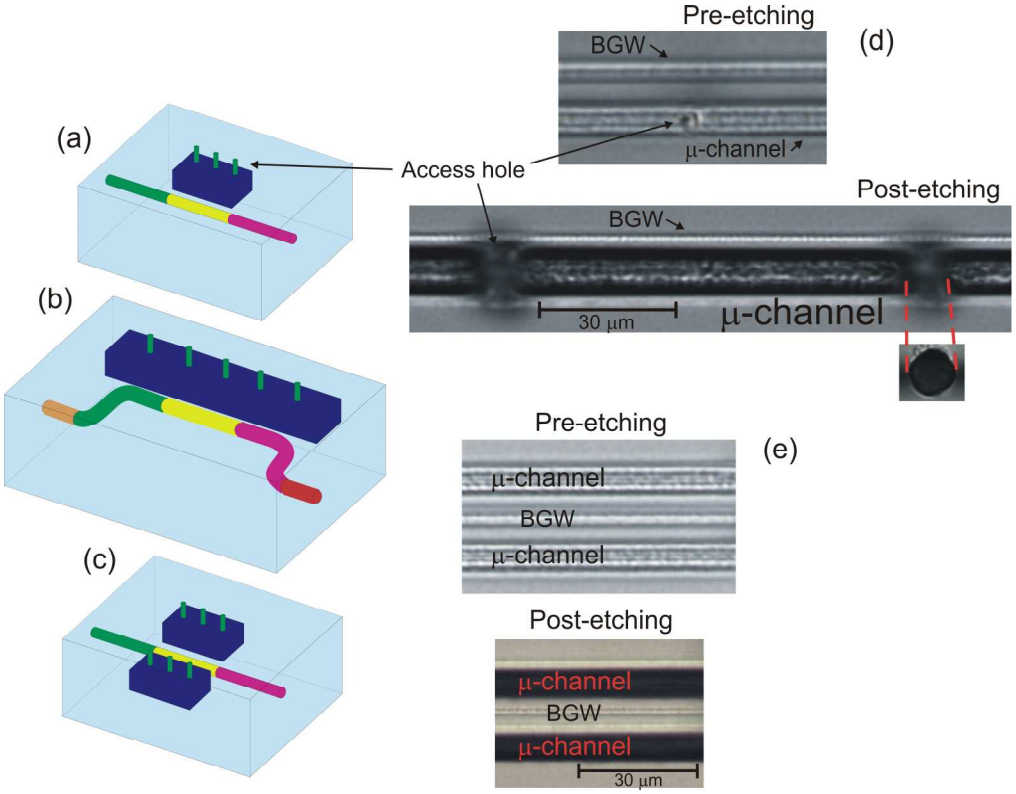

Fig. 2. Schematics of microfluidic sensor geometries: straight BGW single channel (a), S-bend BGW single channel (b), and straight BGW double channel (c). Microscope images recorded before (top pictures in (d) and (e)) and after (bottom pictures in (d) and (e)) HF etching for the straight BGW single channel (d) and the straight BGW double channel (e) sensor designs.

The second sensor geometry, shown in Fig. 2(b), consisted of a double S-bend waveguide positioned with the sensing BGW parallel to and slightly shorter than the adjacent microchannel. With this configuration, the sensor grating does not probe the starting and ending walls of the channel that induce back reflections and spectral distortions to the Bragg resonance. Lower waveguide losses are anticipated as the bending waveguide arm approaches the channel adiabatically without abrupt change in the propagation constant or the mode profile at the channel end point [16]. Radii of curvature in the 10 to 50 mm range were tested. Although bend losses increased slightly with smaller radius in this range, all radii yielded very similar spectral response and 10 mm radius was selected for a more compact layout. An insertion loss (IL) of ~-4 dB was measured, which was similar to the IL of the straight BGW geometry in Fig. 2(a). The S-bend waveguide (Fig. 2(b)) was separated into five wavelength segments: $\lambda_3 = 1560$ nm for refractive index sensing (yellow); $\lambda_1 = 1545$ nm and

#111972 - $15.00 USD Received 27 May 2009; revised 11 Jun 2009; accepted 23 Jun 2009; published 26 Jun 2009

λ_5 = 1550 nm (orange and red, respectively) for temperature and/or strain gauging; and λ_2 = 1530 nm and λ_4 = 1540 nm (green and pink, respectively) to serve as the bend arms where chirping and other spectral distortions were kept far outside of the sensor (λ_3) spectral band. The channel was 15 mm long and formed with ~1 μm channel-to-BGW separation.

The arrangement in Fig. 2(c) is an extension of Fig. 2(a) that places two identical channels parallel to and on opposite sides of the sensor BGW. The objective is to increase the amount of evanescent field that penetrates into the microfluidic channels and thus improve the device sensitivity. The BGW wavelengths and channel lengths were the same as for the topology of Fig. 2(a). The microscope image in Fig. 2(e) shows the two microchannels positioned with ~2 μm gaps on either side of the BGW.

4. Refractive index sensing

After HF etching, the glass facets were ground and polished to access the waveguides for spectral characterization. Infrared light from a randomly polarized broadband source (Thorlabs ASE-FL7002, 1530 nm to 1610 nm) was routed through an optical fiber circulator and coupled into the BGWs with a single-mode fiber. Another single-mode fiber was aligned to the exit facet of the waveguides to guide the transmitted light to an optical spectrum analyzer (OSA; Ando AQ6317B, with 0.01 nm resolution) for recording transmission spectra. The reflected light from the BGWs was passed back to the optical circulator and guided to the OSA for reflection responses. Index matching fluid was used at both waveguide-fiber interfaces to reduce Fresnel reflections and Fabry-Perot effects. The transmission spectra were normalized relative to the direct fiber-to-fiber transmission measurement. The reflection spectra were normalized against the power returned by a high reflection fiber reflector and corrected with the known reflectivity R = 96%.

Spectral shifts in the Bragg resonant wavelength were induced by filling the channels with distilled white vinegar (5% acetic acid; n_D = 1.333). Droplets placed on the vertical entrance holes were drawn in by capillary forces to the buried channel. Refractive index matching oils (Cargille) were also introduced with the following n_D values: 1.402, 1.442, 1.444, 1.448, and 1.452. The chip was rinsed in an ultrasonic bath of acetone and then dried before the next fluid was filled.

Bragg grating reflection spectra are shown in Fig. 3(a) for the double channel sensor of Fig. 2(c), for air (blue; n_D = 1.000) and index oil (red; n_D = 1.444) filling the channels. A 0.7 nm wavelength shift is clearly evident here due to the Δn = 0.444 change in refractive index. A larger wavelength shift was limited by the 2 μm wide gap between BGW and channels. In contrast, no detectable spectral shift is observable for the λ_3 = 1550 nm reference grating wavelength, which does not sample the channel fluids, as shown in Fig. 3(b). This reference resonance presented the narrowest ($\Delta\lambda \approx$ 0.22 nm at 3 dB) and strongest (~25 dB contrast) Bragg response and lowest loss (~-0.14 dB) relative to the corresponding values for the 1560 nm BGW of $\Delta\lambda \approx$ 0.36 nm, ~23 dB contrast and ~-6.7 dB loss. This spectral degradation increases as the BGW is positioned closer to the channel due to wall roughness and gap non-uniformity, which cause higher scattering loss and spectral broadening. In order to improve the precision in finding the centre wavelength of the Bragg reflection peak, all spectral data were fitted to a Gaussian function.

#111972 - $15.00 USD Received 27 May 2009; revised 11 Jun 2009; accepted 23 Jun 2009; published 26 Jun 2009

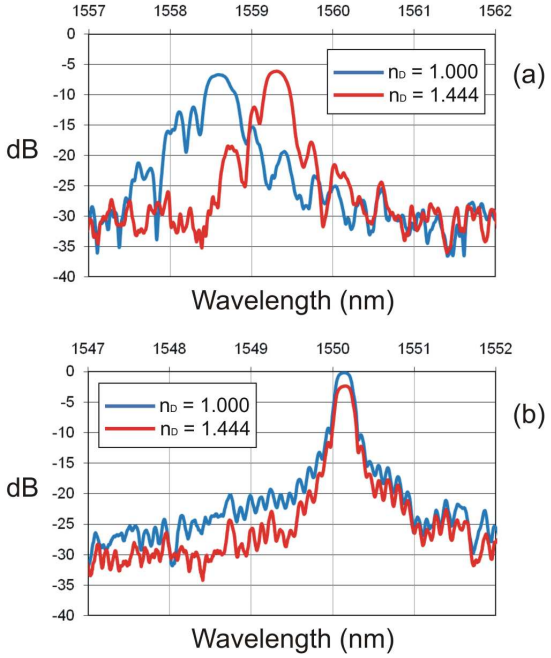

Fig. 3. Bragg grating reflection spectra for (a) the 1560 nm sensing grating and (b) the 1550 nm reference grating, for microchannels filled with air ($n_D = 1.000$) and index matching oil ($n_D = 1.444$). The sensor geometry of Fig. 2(c) was used.

The resonance wavelength of all the BGWs is known to shift both with strain and temperature, as previously reported in [35]. However, strain effects due to sample mountings were too small to affect present observations. Changes in the laboratory temperature (± 1°C) induced shifts in reference and sensing grating resonances that followed the thermo-optic response [36]:

$$\Delta\lambda_B / \lambda_B = \Delta T /(\alpha + \zeta) \qquad (2)$$

where α = 0.55×10^{-6} °C^{-1} is the thermal expansion coefficient for fused silica glass and ζ = 6.16×10^{-6} °C^{-1} is the thermo-optic coefficient measured for BGWs [35]. This thermo-optic response is similar to the ζ = 8.6×10^{-6} °C^{-1} value reported for a single-mode fiber [37].

For an OSA resolution of $\Delta\lambda$ = 0.01 nm, Eq. 2 predicts a temperature change $\Delta T \approx 0.7$ K (at λ_B = 1550 nm), which is similar to the ± 1°C laboratory temperature fluctuation. To improve the accuracy of refractive index measurement, temperature variations in the substrates were accounted by subtracting the temperature-only induced shift observed for the reference gratings from the wavelength shift measured by the sensor grating. This compensation improved the precision of the present data only modestly but such techniques are essential for microreactors and other field use where temperature migrations exceed ± 1°C.

Figure 4 plots the measured Bragg resonance wavelength, corrected for temperature fluctuations, against the refractive index of the solvents filling the microchannels. Each of the three device configurations are presented for the most sensitive device tested (*i.e.*, with the smallest BGW-to-channel separation). The slope of these curves represents the refractive index sensitivity (nm/riu) and is plotted in Fig. 5. The highest sensitivity values were 55 nm/riu, 40 nm/riu and 81 nm/riu, respectively, for the single channel, S-bend waveguide and double channel designs. Given the present minimum λ shift of 0.01 nm resolvable by the

#111972 - $15.00 USD Received 27 May 2009; revised 11 Jun 2009; accepted 23 Jun 2009; published 26 Jun 2009

OSA, the 81 nm/riu response offers a minimum resolvable refractive index variation Δn_{min} of ~1.2×10^{-4}. The highest sensitivity is obtained when the refractive index of the oil filling the channel approaches the value of the fused silica substrate (n_D = 1.458). At higher refractive index, waveguide propagation losses increase dramatically as light spills out into the fluid-filled channel.

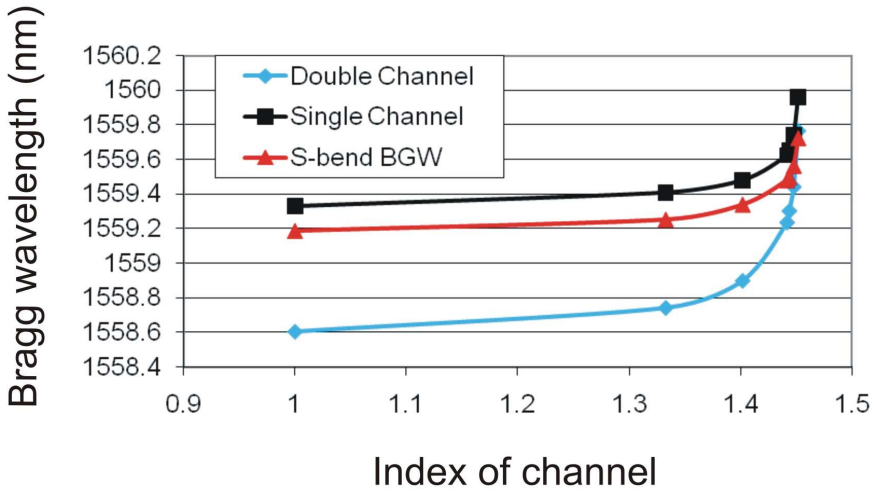

Fig. 4. Bragg resonance values for the sensing grating recorded as a function of the refractive index of the solvents filling the microchannels, for each of the three device configurations presented in Fig. 2.

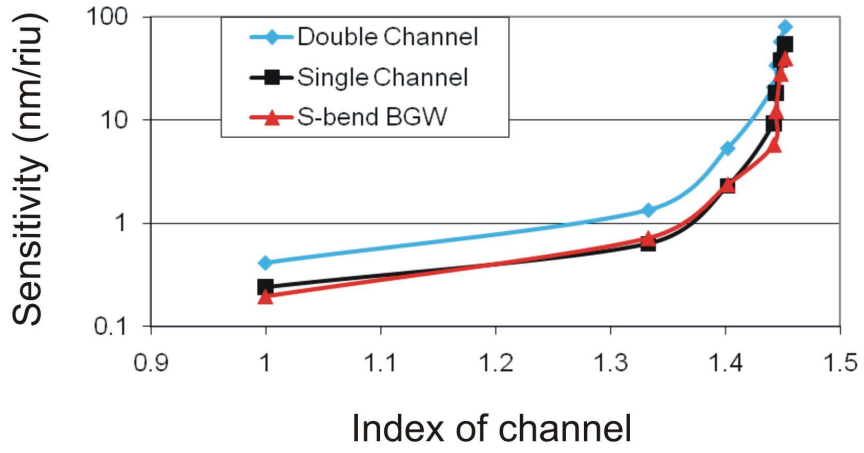

Fig. 5. Refractive index sensitivity *versus* the refractive index of the solvents filling the microchannels, for each of the three device configurations presented in Fig. 2.

As noted in section 2.3, an important trade-off for improving the device sensitivity is increasing the evanescent field in the channel with a thinner BGW-to-channel gap, without imposing strong scattering losses or broadened Bragg resonances. Figure 6 shows the fall off in the waveguide measured insertion loss as this gap thickness was decreased from 3.3 μm to

#111972 - $15.00 USD Received 27 May 2009; revised 11 Jun 2009; accepted 23 Jun 2009; published 26 Jun 2009

1.5 μm for the straight waveguide single channel sensor design. The testing medium dramatically reduces losses by orders of magnitude (>20 dB for the smallest BGW-to-channel distance) as the refractive index increases from n_D = 1.000 to n_D = 1.442. These are expected trends as closer BGWs are more affected by the stronger light intensity that scatters from the channel wall when increasing the refractive index contrast (decreasing n_D). The limit is reached when the n_D value equals or exceeds the fused silica one. The reported IL values were measured at λ = 1563 nm, outside the range of Bragg grating radiation mode losses.

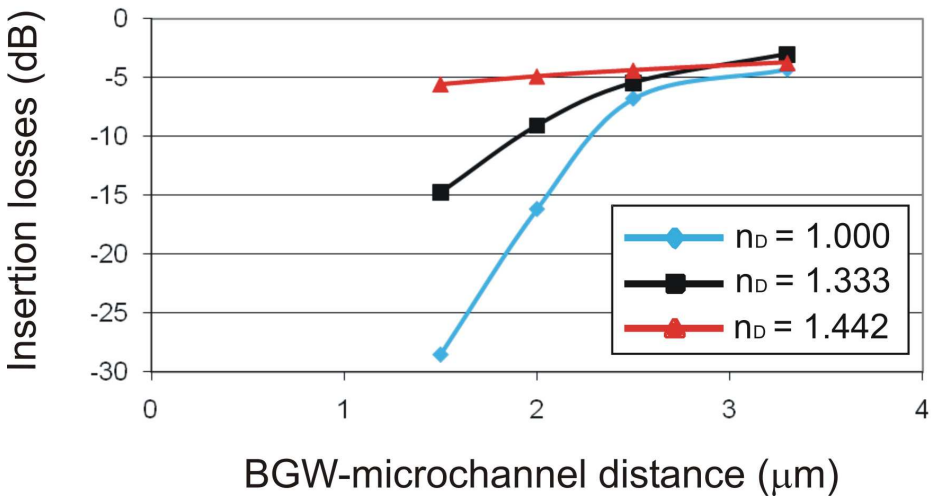

Fig. 6. Experimental BGW insertion losses plotted against BGW-to-microchannel distance for a channel filled with air (n_D = 1.000), distilled white vinegar (n_D = 1.333), and 1.442 index matching oil. The sensor geometry of Fig. 2(a) was used.

On comparing the sensitivity of the three BGW sensor designs (Fig. 5), the dual channel sensor was ~1.5 times more sensitive than the straight waveguide single channel sensor. A two-fold increase in sensing strength was not observed due to the imprecise HF etching that placed the waveguide slightly off-centre (~0.6 μm) between the microchannels. The S-bend Bragg grating waveguide sensor provided a sensitivity similar to the straight BGW single channel design one. Both designs follow a similar dependence on BGW-to-channel gap and channel roughness, which dominated over the advantages related to avoiding the channel edge effects discussed above.

Temperature compensation of the BGW sensors was tested by epoxy-bonding optical fibers to the double channel device and monitoring Bragg wavelength shifts of the reference and sensor gratings, for air- and distilled water-filled channels, as the substrate was heated on a hotplate in the 25°C to 125°C range. The wavelength shifts were linear with temperature, yielding $\lambda_{125°C}$ - $\lambda_{25°C}$ values of 1.17 nm and 1.34 nm for the sensor and the reference grating, respectively, for the case of air-filled channels. For water-filled channels (n_D = 1.333) a linear response was also noted in the 25°C to 75°C range, with $\lambda_{75°C}$ - $\lambda_{25°C}$ shifts of 0.4 nm and 0.6 nm observed for the sensor and the reference grating, respectively. Only by subtracting the reference grating wavelength shifts from the corresponding sensor values could the temperature response of the grating be removed and an accurate high temperature reading of the refractive index be provided. This feature of temperature compensation is essential when integrating such BGW devices into 3D optofluidic microsystems for optical sensing of gases, liquids, and biological media. Similar methods can be applied for strain compensation as expected when temperature gradients in exothermic microreactors or stresses in multi-layered LOC devices arise [35].

#111972 - $15.00 USD Received 27 May 2009; revised 11 Jun 2009; accepted 23 Jun 2009; published 26 Jun 2009

5. Conclusions

This paper presents, to our best knowledge, the first example of integrating Bragg grating waveguides and microfluidic channels, both fabricated on a commercial fused silica glass substrate by means of femtosecond laser exposure and chemical etching. By writing the BGWs sufficiently close to the microchannels, evanescent probing of the waveguide mode into the liquid-filled channel enabled refractive index sensing in the 1 to 1.452 range with a maximum sensitivity of 81 nm/riu or minimum detectable index change of ~1.2×10^{-4}. Improvements to the channel wall roughness together with the extension of channels to wrap fully around the BGW promise even larger sensitivity response such as the 1394 nm/riu value demonstrated in an etched fiber Bragg grating sensor [15]. Further improvements are anticipated by narrowing the Bragg resonance linewidth with shorter length BGWs or engineering spectral defects with π-phase shifts.

The present methods permit BGW sensors to be flexibly integrated into planar or 3D lab-on-chip devices for optofluidic sensing applications emerging in microreactors for chemical synthesis and monitoring of biomolecular interactions. Compensation for temperature variation together with the general prospects for 3D distributed sensing of temperature, strain, and refractive index are new key opportunities for developing the next generation of optofluidic microsystems.

Acknowledgements

Financial support from the Canadian Institute for Photonics Innovation and the Natural Sciences and Engineering Research Council of Canada is gratefully acknowledged.

#111972 - $15.00 USD Received 27 May 2009; revised 11 Jun 2009; accepted 23 Jun 2009; published 26 Jun 2009